JOURNAL OF CHEMICAL INFORMATION AND MODELING

Article

pubs.acs.org/jcim

Discovery of Novel and Selective Adenosine A_{2A} Receptor Antagonists for Treating Parkinson's Disease through Comparative Structure-Based Virtual Screening

Sheng Tian,[†,∥] Xu Wang,[†,∥] Linlang Li,[†,∥] Xiaohu Zhang,[†] Youyong Li,[§] Feng Zhu,[‡] Tingjun Hou,*[,‡] and Xuechu Zhen*[,†]

[†]Jiangsu Key Laboratory of Translational Research and Therapy for Neuropsychiatric Diseases and College of Pharmaceutical Sciences, Soochow University, Suzhou, Jiangsu 215123, China

[‡]College of Pharmaceutical Sciences, Zhejiang University, Hangzhou, Zhejiang 310058, China

[§]Institute of Functional Nano & Soft Materials (FUNSOM), Soochow University, Suzhou, Jiangsu 215123, China

Supporting Information

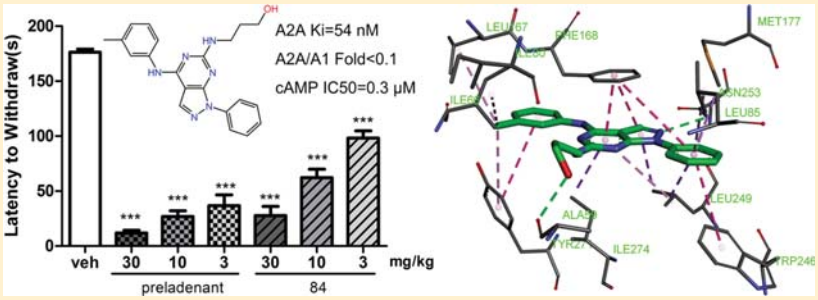

ABSTRACT: Among non-dopaminergic strategies for combating Parkinson's disease (PD), antagonism of the A_{2A} adenosine receptor (AR) has emerged to show great potential. In this study, on the basis of two crystal structures of the A_{2A} AR with the best capability to distinguish known antagonists from decoys, docking-based virtual screening (VS) was conducted to identify novel A_{2A} AR antagonists. A total of 63 structurally diverse compounds identified by VS were submitted to experimental testing, and 11 of them exhibited substantial activity against the A_{2A} AR (K_i < 10 μM), including two compounds with K_i below 1 μM (compound **43**, 0.42 μM; compound **51**, 0.27 μM) and good A_{2A}/A_1 selectivity (fold < 0.1). Compounds **43** and **51** demonstrated antagonistic activity according to the results of cAMP measurements (cAMP IC_{50} = 1.67 and 1.80 μM, respectively) and showed good efficacy in the haloperidol-induced catalepsy (HIC) rat model for PD at doses of up to 30 mg/kg. Further lead optimization based on a substructure searching strategy led to the discovery of compound **84** as an excellent A_{2A} AR antagonist (A_{2A} K_i = 54 nM, A_{2A}/A_1 fold < 0.1, cAMP IC_{50} = 0.3 μM) that exhibited significant improvement in anti-PD efficacy in the HIC rat model.

INTRODUCTION

Parkinson's disease (PD) is a chronic neurodegenerative disorder that affects about 1% of the population over the age of 65.[1−3] The treatments for PD are primarily based on dopaminergic replacement strategies to restore dopamine functions. These dopamine-targeted therapies provide symptomatic relief of the PD-related motor disturbances but do not alter the disease process. In addition, with continued treatment, these drugs show reduced efficacy and produce undesirable side effects, including on−off effects, hallucination, and dyskinesia.[4−6] Furthermore, the currently available dopaminergic drugs have very limited effects for the treatment of nonmotor symptoms that frequently accompany PD, such as mood, postural instability, and cognitive disturbances.[1,7] Therefore, there is an urgent need to develop effective and durable symptom- and disease-modifying therapies for the long-term management of PD.

Among non-dopaminergic strategies for the treatment of PD, pharmacological blockade of the A_{2A} adenosine receptor (AR) has received considerable attention in the past decade.[8−12] Adenosine is an important neuromodulator that exerts its functions through interactions with the A_1, A_{2A}, A_{2B}, and A_3 AR subtypes, which belong to the G-protein-coupled receptor (GPCR) superfamily. In the striatum, the A_{2A} AR colocalizes and associates with the dopamine D_2 receptor physically. A_{2A} AR antagonists enhance D_2-dependent signaling by inducing immediate early gene c-fos expression in the striatopallidal pathway and facilitate other D_2-mediated responses.[13] Moreover, a number of A_{2A} AR antagonists have been shown to normalize motor function in animal models of PD without inducing dyskinesia.[14]

Received: April 4, 2017
Published: May 2, 2017

DOI: 10.1021/acs.jcim.7b00188
J. Chem. Inf. Model. 2017, 57, 1474−1487

Representative A_{2A} AR antagonists that have progressed into clinical trials are shown in Figure 1. Istradefylline (KW-6002),[15]

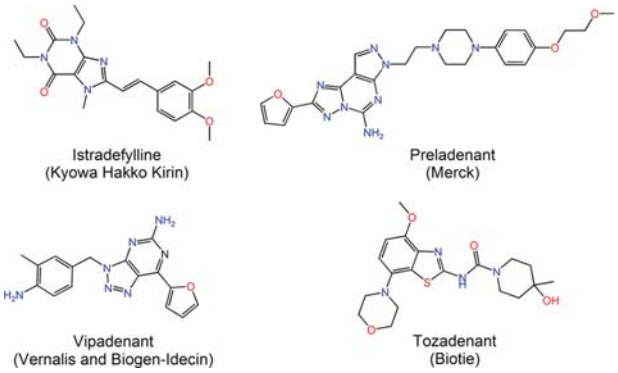

Figure 1. Chemical structures of four representative A_{2A} AR antagonists.

which has shown efficacy in numerous preclinical models of PD, is the most advanced A_{2A} AR antagonist. In 2013, istradefylline was approved for clinical use in Japan as the adjunctive treatment for PD. This breakthrough, along with other advances in preclinical/clinical studies, has boosted interest in finding more promising A_{2A} AR antagonists for the treatment of PD.[8,9,16]

Although a number of promising A_{2A} AR antagonists with good affinity and selectivity have been identified successfully by using structural optimizations/modifications, most of them, such as purine and xanthine derivatives, generally have high molecular weights, contain a furan group that is prone to oxidative metabolism, and have limited structural diversity.[8,16−19] Consequently, there remains an ongoing need to find promising antagonists of the A_{2A} AR with novel scaffolds.

Virtual screening (VS), especially structure-based VS, has been widely used in hit identification.[20−24] To date, there have been several attempts to identify potent A_{2A} AR antagonists by using docking-based VS based on protein structures derived from homology modeling or experimentally determined crystal structures of the A_{2A} AR.[25−30] In 2010, using the crystal structure of the A_{2A} AR (PDB ID 3EML[31]), Carlsson and co-workers identified seven A_{2A} AR antagonists with affinities between 200 nM and 9 μM through docking-based VS, and the most potent candidate is structurally novel and has good selectivity for the A_{2A} subtype versus the A_1 and A_3 subtypes.[25] Similarly, using the A_{2A} AR crystal complex (PDB ID 3EML[31]), Katritch et al.[26] identified 23 A_{2A} AR antagonists with affinities (K_i) below 10 μM, and 10 hits were proved to be A_{2A} AR antagonists by functional assays. It needs to be pointed out that almost all structure-based VS for A_{2A} AR has been carried out using the same A_{2A} AR crystal complex (PDB ID 3EML[31]) or A_{2A} AR structures generated from homology modeling.[25−28] Previous studies showed that the predictions of molecular docking based on different structures of the same target may be quite different because the binding patterns characterized by these different complexes are varied.[32−38] Therefore, comparing the performances of docking-based VS based on different protein crystal structures for a specific target and using the reliable crystal templates to screen commercial databases seems to be a more reasonable approach to identify promising active compounds.

In the current study, on the basis of nine available crystal structures of the A_{2A} AR, the performances of docking-based VS for all of the crystal structures were compared by using two independent validation data sets (VD1 and VD2). Then the two A_{2A} AR crystal complexes with the best discrimination power for VS were used to identify 61 potential A_{2A} AR ligands with diverse chemical structures from the ChemDiv database, which were submitted to experimental testing. Eleven of them exhibited significant binding activity against the A_{2A} AR (A_{2A} K_i < 10 μM), including the two most potent hits with K_i below 1 μM (compound **43**, 0.42 μM; compound **51**, 0.27 μM), which were also confirmed as functional A_{2A} AR antagonists. Furthermore, these two hits exhibited reasonable selectivity over the A_1 AR (A_{2A}/A_1 fold < 0.1). In addition, when dosed at 30 mg/kg, compounds **43** and **51** showed satisfactory efficacy in the haloperidol-induced catalepsy (HIC) rat model for PD. Finally, substructure searching was applied to discover more promising antagonists of the A_{2A} AR based on the core scaffolds of compounds **43** and **51**. Several potent A_{2A} AR antagonists were found in the 12 analogues of compound **43** and 20 analogues of compound **51**, and the most promising candidate, compound **84**, demonstrated excellent A_{2A} AR antagonist activity (A_{2A} K_i = 54 nM; cAMP IC_{50} = 0.3 μM), good selectivity (A_{2A}/A_1 fold < 0.1), and good efficacy in the HIC rat model for PD at three doses (3, 10, and 30 mg/kg).

MATERIALS AND METHODS

Preparation of Crystal Structures and Validation Data Sets. The crystallographic structures of the A_{2A} AR in complex with antagonists were retrieved from the RCSB Protein Data Bank (PDB).[39] To date, nine crystal structures of A_{2A} AR−antagonist complexes have been released, including PDB IDs 3EML,[31] 3RFM,[40] 3REY,[40] 3PWH,[40] 3VG9,[41] 3VGA,[41] 3UZA,[27] 3UZC,[27] and 4EIY.[42] For each complex, the *Protein Preparation Wizard* module in Schrödinger 9.0[7] was used to remove all crystallographic water molecules, add missing side chains and hydrogen atoms, assign protonation states and partial charges with the OPLS2005 force field, and minimize the whole crystal structure until the root-mean-square deviation (RMSD) of the displacement of the non-hydrogen atoms reached ≤0.3 Å.

Two independent validation data sets for decoys were used to evaluate the performance of docking-based VS based on different crystal structures.[34,35,43] Validation data set 1 (VD1) was directly extracted from the GPCR decoy database (GDD) compiled by Gatica and Cavasotto.[44] In the spirit of GDD, for each A_{2A} AR antagonist, 39 decoys were selected from the ZINC database,[45] ensuring the similarity of six physiochemical properties (molecular weight, formal charge, hydrogen bond donors/acceptors, rotatable bonds, and log*P*) but structural dissimilarity (Tanimoto coefficient < 0.75). As reported by Krüger and Evers,[46] the use of commercial databases is also an effective way to represent the chemical space of a decoy set. Validation data set 2 (VD2) was also employed in our study. For each A_{2A} AR antagonist deposited in the GDD, 39 decoys were randomly selected from the ChemDiv database on the basis of the two-dimensional (2D) similarity (Tanimoto coefficient) of the FCFP_4 fingerprints using the *Find Diverse Molecules* protocol in Discovery Studio 3.1 (DS3.1).[6] At last, VD1 had 361 antagonists and 14 079 decoys from ZINC, and VD2 had 361 antagonists and 14 079 decoys from ChemDiv.

Comparative Docking-Based Virtual Screening. Prior to VS, the performances of molecular docking based on different A_{2A} AR complex structures were investigated systematically. All of the chemicals in VD1 and VD2 were processed

DOI: 10.1021/acs.jcim.7b00188
J. Chem. Inf. Model. 2017, 57, 1474−1487

using the *LigPrep* module in Schrödinger.[7] For each antagonist or decoy, the ionized states and tautomers/stereoisomers were generated using *Epik* at pH = 7.0. For the known antagonists of the A_{2A} AR with 3D structures, the original chiralities were preserved, and for the decoys without 3D structures, different combinations of chiralities were generated. The maximum number of stereoisomers for each decoy was set to 32, and the other parameters for *Ligprep* were set to the default values. Finally, the number of prepared antagonists of the A_{2A} AR was 380, and the numbers of decoys for VD1 and VD2 were 14 681 and 14 173, respectively.

Next, by means of the *Receptor Grid Generation* component of *Glide* in Schrödinger, the binding pocket with the size of 10 Å × 10 Å × 10 Å was defined for each A_{2A} AR complex and centered on the center of mass of the cocrystallized antagonist. The default settings in *Glide* were used for grid generation. All of the chemicals in the two validation data sets were docked into the binding pockets of the nine A_{2A} AR complexes and scored using the standard precision (SP) and extra precision (XP) scoring functions of *Glide*. Five thousand poses per chemical were generated during the initial phase of docking, out of which the best 400 poses were selected for energy minimization by 100 steps of conjugate-gradient minimizations with a dielectric constant of 2.0. The performances of the Glide SP and XP scoring functions for the nine A_{2A} AR complexes were evaluated and compared.

All of the compounds in the ChemDiv database were screened against two A_{2A} AR crystal complex structures (3PWH and 4EIY). For all of the compounds in ChemDiv, the ionized states and tautomers were generated at pH 7.0 ± 2.0 using *Epik*. Besides, the different combinations of chiralities were also generated by setting the maximum number of stereoisomers for each compound in ChemDiv to 32. At last, the final VS library had more than 2.65 million compounds. For each complex, the ChemDiv compounds were docked and scored by high-throughput virtual screening (HTVS) scoring of *Glide* first, and the 100 000 top-ranked compounds were retained. Then the saved compounds were redocked into 3PWH or 4EIY using the SP scoring function of *Glide*, and the 10 000 top-ranked compounds were redocked and scored using the XP scoring function of *Glide*.

The nonduplicated top-ranked 1000 chemicals scored by the XP scoring function of *Glide* for each A_{2A} AR complex were evaluated by Lipinski's rule of five,[47] the drug-likeness filter developed in our group,[48,49] and the rapid elimination of swill (REOS)[50] filters to remove non-drug-like molecules and molecules with toxic, reactive, or undesirable groups. Then the remaining compounds were structurally clustered into 100 clusters on the basis of the Tanimoto coefficients computed using the MACCS structural keys, and the compound with the lowest docking score in each cluster was chosen. At last, 63 chemicals were eventually purchased from ChemDiv and tested experimentally.

Initial Pharmacological Screening in Vitro. The purchased compounds were dissolved in 100% dimethyl sulfoxide to a stock concentration of 10 mM. The initial binding assay was conducted at a final concentration of 100 μM for each compound. Competition binding was performed using stably transfected A_{2A}R-HEK293 cell membrane with [^{3}H]-ZM241385 (50.00 Ci/mmol ART 0884) at a final concentration of 0.1 nM to detect specific binding as previously described by us.[16] Nonspecific binding was examined using 5′-*N*-ethylcarboxamidoadenosine (NECA) at a concentration of 10 μM. The hit compounds capable of inhibiting no less than 80% were determined.

A_{2A} AR Membrane Binding. Each compound that elicited more than 80% inhibition of receptor binding as described above was further subjected to a binding affinity assay to measure the K_i value. Membranes were obtained from stable A_{2A}R-HEK293 cells grown on 100 mm × 20 mm plates in 5% CO_2 at 37 °C. At 95% confluence, cells were washed twice with cold phosphate-buffered saline (DPBS). After 1 mL of DPBS was added, the cells were collected into 1.5 mL tubes and centrifuged for 10 min at 1000*g*. The cell pellet was resuspended and homogenized in 250 μL of cold lysis buffer (50 mM Tris, pH 7.4, 2 mM EDTA, protease inhibitor mixture) and then centrifuged for 10 min at low speed (100*g*). The supernatant was transferred to new cold 1.5 mL microcentrifuge tubes and centrifuged at 30000*g* for 20 min at 4 °C. The pellet was frozen at −80 °C for later use or resuspended in cold binding buffer (50 mM Tris, pH 7.4, 100 mM NaCl) for immediate use in a membrane-binding assay. The protein content was determined using the BCA protein assay. For competition binding, A_{2A}R-HEK293 membranes were incubated at room temperature with [^{3}H]ZM241385 radioligand (0.1 nM) and the nonradioactive competitor NECA with increasing concentrations from 1 nM to 100 μM or 10 μM to measure nonspecific binding. Reactions were carried out in 12 mm × 75 mm borosilicate glass tubes at 37.5 °C for 30 min and terminated by rapid filtration through a 12-well filter plate (Millipore, USA) equipped with Whatman GF/B filter papers. The filters were washed and dried. Radioactivity was determined using a Beckman LS-6500 counter (PerkinElmer, Waltham, MA, USA). Data were analyzed with GraphPad Prism 5.0 software. IC_{50} values were generated and converted to K_i values using the Cheng−Prusoff equation ($K_i = IC_{50}/[1 + ([L]/K_d)]$).

Adenosine A_1 Receptor Membrane Binding. Compound binding affinities for the A_1 AR were tested to verify selectivity. Competition binding assays were performed using A_1 AR-expressing HEK293 cells. Cells were cultured and membranes were obtained according to the methods described previously.[16,18,19] For competition binding, A_1R-HEK293 cell membranes were incubated for 30 min with [^{3}H]DPCPX (0.3 nM) and either nonradioactive competitor (1 nM to 100 μM) to assess nonspecific binding of the A_1 AR. The reactions were carried out using the same protocol as for A_{2A} AR membrane binding.

cAMP Functional Assay. A cAMP functional assay was performed using stably transfected A_{2A}R-HEK293 cells. When cells were grown to about 85% confluence on 100 mm × 20 mm plates, they were washed and detached with 0.25% Trypsin-PBS solution. Then the cells were collected at 1100 rpm for 3 min at room temperature and resuspended in Hank's balanced salt solution (138 mM NaCl, 5 mM KCl, 1.3 mM $CaCl_2$, 0.5 mM $MgCl_2$, 0.4 mM $MgSO_4$, 0.3 mM KH_2PO_4, 0.3 mM Na_2HPO_4, 5.6 mM glucose, pH 7.4) containing 100 μM 3-isobutyl-1-methylxanthine (Sigma, cat. no. I7018) as a phosphodiesterase inhibitor. The cells were loaded into 384-well plates (~4000 cells/well) and preincubated with tested compound (1 nM to 100 μM) for 30 min at room temperature, followed by addition of 100 nM NECA. After 10 min at room temperature, the cAMP concentration was measured according to the manufacturer's instructions for the cAMP kit as described recently.[51] IC_{50} values were determined from the concentration−response curves (GraphPad Prism 5.0) after log transformation.

DOI: 10.1021/acs.jcim.7b00188
J. Chem. Inf. Model. 2017, 57, 1474−1487

Table 1. Docking Power and Discrimination Power of *Glide* Docking for the Nine A_{2A} AR−Antagonist Complexes for VD1 and VD2

		docking power (RMSD/Å)		discrimination power (P value)			
				VD1		VD2	
PDB ID	ligand	SP	XP	SP	XP	SP	XP
3EML	ZMA	2.86	9.13	6.96×10^{-72}	5.46×10^{-46}	8.08×10^{-72}	5.07×10^{-59}
3RFM	caffeine	3.05	3.96	7.33×10^{-44}	2.68×10^{-41}	1.05×10^{-36}	1.47×10^{-42}
3REY	XAC	7.09	5.62	2.88×10^{-45}	2.70×10^{-24}	3.16×10^{-38}	1.85×10^{-21}
3PWH	ZMA	2.60	2.31	1.65×10^{-89}	6.21×10^{-63}	4.59×10^{-92}	6.02×10^{-68}
3VG9	ZMA	4.14	5.61	4.36×10^{-31}	1.50×10^{-14}	6.09×10^{-37}	2.85×10^{-25}
3VGA	ZMA	1.92	1.90	5.12×10^{-39}	3.40×10^{-32}	1.96×10^{-40}	1.80×10^{-37}
3UZA	T4G	0.50	0.46	1.47×10^{-46}	2.24×10^{-48}	6.71×10^{-37}	1.37×10^{-38}
3UZC	T4E	1.67	1.65	2.33×10^{-60}	3.22×10^{-54}	6.65×10^{-45}	3.92×10^{-50}
4EIY	ZMA	1.55	3.66	2.65×10^{-94}	1.42×10^{-52}	5.94×10^{-89}	2.67×10^{-55}

Behavioral Testing. Catalepsy was induced by haloperidol in male Wistar rats (180−220 g). Haloperidol was administered intraperitoneally (i.p.) 1 h prior to the tested compounds. One hour after i.p. drug administration, the behavioral test trial (maximum duration of 180 s) was begun by placing the forepaws of rats on a 10 cm high bar (horizontally placed) and their hindquarters on a platform. The time was recorded when the animal fully removed both paws from the bar or climbed onto the bar with all of its limbs as described previously.[16,51]

Substructure Searching. The substructure searching function embedded in Molecular Operating Environment (MOE)[25] was utilized to find the analogues with the core scaffold architectures (Murcko framework)[52] of the two promising A_{2A} AR antagonists (compounds **43** and **51**) from the ChemDiv database. For compounds **43** and **51**, 12 and 20 analogues, respectively, were identified and purchased for bioassays.

RESULTS AND DISCUSSION

Performance of Docking-Based Virtual Screening. First of all, the "docking power", which is an important index of docking reliability for reproducing the experimental binding modes of antagonists, was evaluated. For each A_{2A} AR complex, the antagonist was extracted from the crystal structure and then redocked into the respective binding pocket. The RMSD between the docked pose and the original conformation of the antagonist for each complex was calculated, and RMSD $\leq$ 2.0 Å was used as the criterion of successful docking. As shown in Table 1, *Glide* docking successfully recognized the near-native conformations of the cocrystallized antagonists for four of the nine A_{2A} AR complexes using the SP or XP scoring function of *Glide*.

Next, the "discrimination powers" of molecular docking to distinguish the known antagonists from the decoys in VD1 and VD2 for the nine complexes of the A_{2A} AR were examined and compared. In comparison with the docking power, the discrimination power is more important for a practical VS campaign. Student's t test was applied to assess the significance of the difference between the means of the two distributions of the *Glide* SP or XP scores for the known antagonists and decoys. As shown in Table 1, we found that *Glide* docking could efficiently distinguish the known antagonists from the decoys in VD1 for the nine complexes, as indicated by the relatively low P values ($<10^{-20}$). The best discrimination power (P value = 2.65×10^{-94}) was obtained using the SP scoring function of *Glide* and 4EIY as the docking template. The distributions of the SP and XP scores with the best discrimination power for each complex are depicted in Figure 2. Besides, *Glide* docking can also achieve satisfactory distinguishing power for VD2 (Table 1 and Figure 3). With 3PWH as the docking template, the best discrimination power can be achieved using the SP scoring function for VD2 ($P = 4.59 \times 10^{-92}$). Our results illustrate that the comparison of the performances of *Glide* docking based on different A_{2A} AR complexes is quite necessary. According to the discrimination power, 4EIY and 3PWH were selected as the initial templates for the *Glide*-docking-based VS.

A_{2A} AR Membrane Binding Assay. A total of 63 potential hits predicted by the docking-based VS based on two A_{2A} AR crystal complexes (4EIY and 3PWH) were purchased. Competition binding assays were performed using stably transfected A_{2A}R-HEK293 cell membranes with [^{3}H]ZM241385 (50.00 Ci/mmol ART 0884). As shown in Table S1 in the Supporting Information, we found that 11 compounds (**6**, **25**, **35**, **37**, **41**, **43**, **47**, **49**, **51**, **61**, and **62**) exhibited over 80% inhibition (hit rate = 17.5%). These 11 compounds were then subjected to the saturation binding assay. As shown in Table 2, the 11 identified compounds exhibit satisfactory binding affinity, with $K_i \lesssim 10$ μM. Among them, two compounds have affinities under 450 nM (compound **43**, 420 nM; compound **51**, 270 nM). The radioligand competition binding curves for compounds **43** and **51** against the A_{2A} AR and a schematic representation of the predicted interactions derived from *Glide* docking between the A_{2A} AR and compound **43** or **51** are depicted in Figure 4.

The chemical structures of the 11 identified ligands of the A_{2A} AR are shown in Figure 5. The structures of these 11 identified A_{2A} AR ligands were compared with the known antagonists of the A_{2A} AR deposited in the BindingDB database.[53] The pairwise similarity (Tanimoto coefficient) of each identified ligand to each known A_{2A} AR antagonist was calculated using the *Find Similarity Molecules by Fingerprints* protocol in DS3.1.[6] The statistical results illustrated that the 11 identified A_{2A} AR antagonists did not share high structural similarity with any known A_{2A} AR antagonist, as indicated by quite low Tanimoto coefficient (~0.35; Table 2). For the two most potent A_{2A} AR ligands, compounds **43** and **51**, the Tanimoto coefficients are only 0.24 and 0.28, respectively. In addition, as shown in Table 2, the 11 identified ligands of the A_{2A} AR have quite desirable physiochemical properties and acceptable ligand efficiencies (better than 0.2 kcal/mol per heavy atom). Finally, it should be noted that for the 11 identified ligands of the A_{2A} AR, five were identified by the *Glide*

DOI: 10.1021/acs.jcim.7b00188
J. Chem. Inf. Model. 2017, 57, 1474−1487

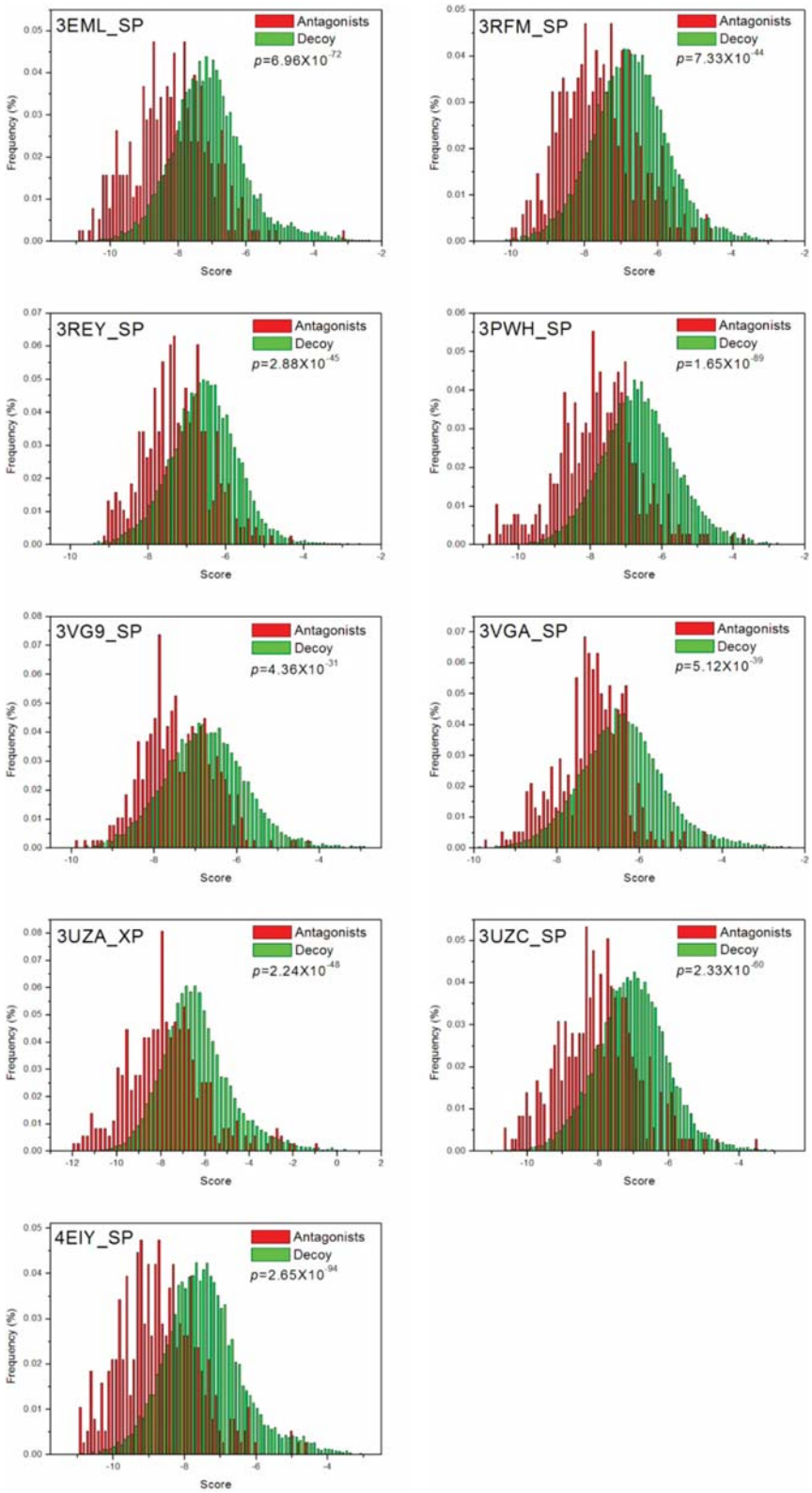

Figure 2. Distributions of the docking scores of VD1 for the nine A_{2A} AR crystal complexes with the best discrimination power.

docking based on 4EIY and six by the *Glide* docking based on 3PWH, suggesting that VS based on different crystal structures is quite necessary. These ligands are structurally novel and may be used as promising leads for further optimizations/modifications.

Adenosine A_{2A}/A_1 Binding Selectivity. In order to examine the A_{2A}/A_1 selectivities of the 11 identified A_{2A} AR ligands, the binding affinities for the A_1 AR were tested. Competition binding assays were performed using

DOI: 10.1021/acs.jcim.7b00188
J. Chem. Inf. Model. 2017, 57, 1474−1487

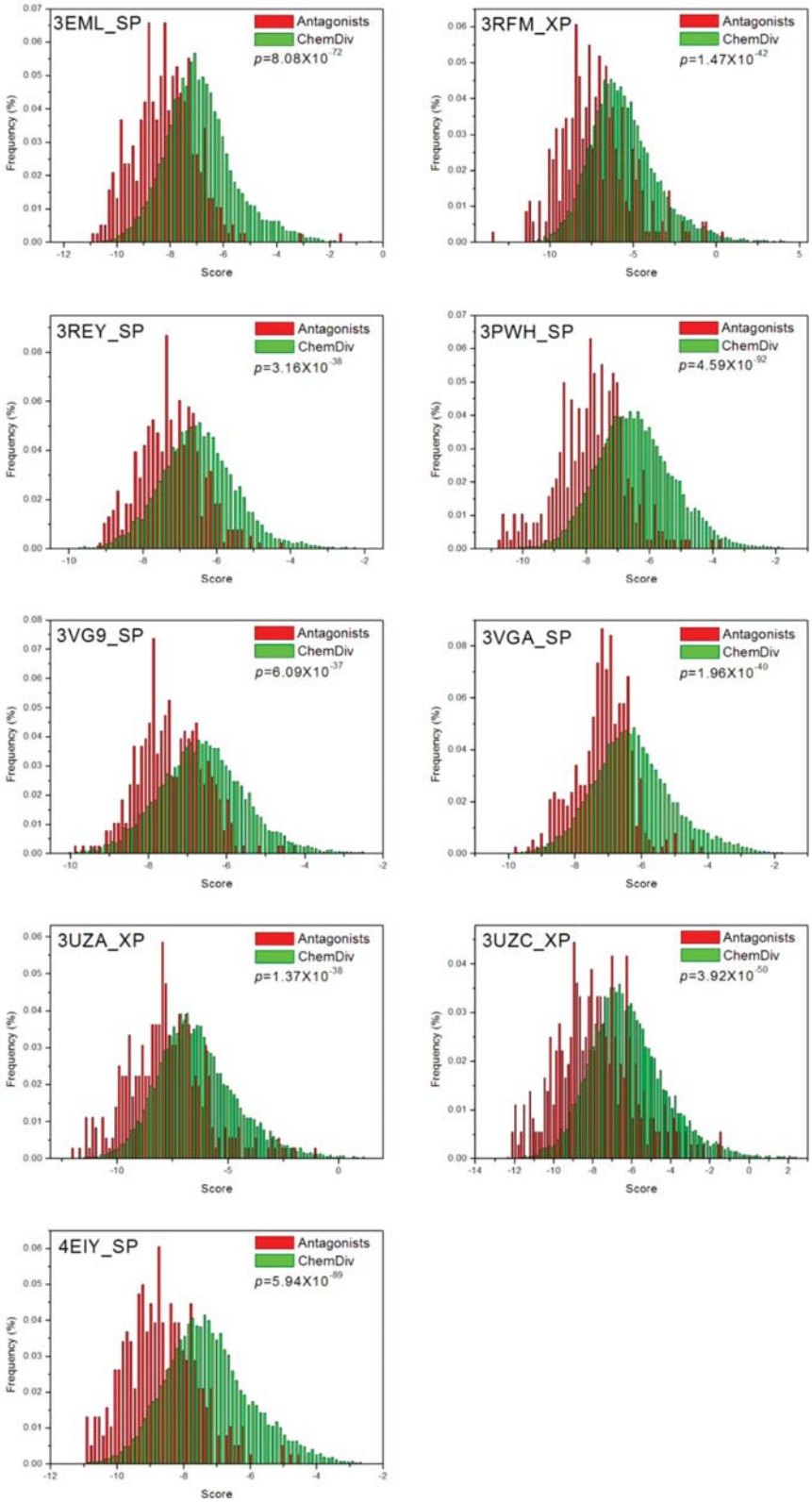

Figure 3. Distributions of the docking scores of VD2 for the nine A_{2A} AR crystal complexes with the best discrimination power.

A_1 AR-expressing HEK293 cells with [^{3}H]DPCPX as described in Materials and Methods. In general, compounds with fold < 0.1 are considered selective for the A_{2A} AR, while those with fold > 10 are considered selective for the A_1 subtype. As shown in Table 2, the A_{2A}/A_1 selectivities for eight compounds (**25**, **35**, **37**, **41**, **43**, **47**, **51**, and **61**) are lower than 0.1, indicating that these compounds are selective for the A_{2A} AR.

DOI: 10.1021/acs.jcim.7b00188
J. Chem. Inf. Model. 2017, 57, 1474−1487

Table 2. Binding Affinities and Representative Molecular Properties of the 11 Identified Ligands of the A_{2A} AR

compd	$K_i \pm$ SEM (μM)[a]			MW[b]	pK_i	log$P$[c]	LE[d]	similarity[e]	template[f]
	A_{2A}	A_1	A_{2A}/A_1						
preladenant	2.18 ± 0.27 (nM)			503.56	8.66				
6	5.49 ± 0.10	4.85 ± 0.94	1.13	422.87	5.26	3.45	0.24	0.24	4EIY
25	2.25 ± 0.15	ND[g]	<0.1	440.50	5.65	5.33	0.23	0.25	3PWH
35	2.97 ± 0.20	ND	<0.1	411.51	5.53	5.93	0.21	0.24	3PWH
37	2.59 ± 0.30	ND	<0.1	469.58	5.59	4.56	0.24	0.25	3PWH
41	3.89 ± 0.28	ND	<0.1	422.49	5.41	5.00	0.23	0.24	3PWH
43	0.42 ± 0.04	6.78 ± 0.47	0.06	425.49	6.38	5.08	0.29	0.24	3PWH
47	3.54 ± 0.03	ND	<0.1	394.48	5.45	5.58	0.25	0.31	3PWH
49	2.89 ± 0.34	1.87 ± 0.42	1.55	395.51	5.54	3.33	0.30	0.35	4EIY
51	0.27 ± 0.06	ND	<0.1	333.39	6.57	5.36	0.26	0.28	4EIY
61	10.47 ± 2.49	ND	<0.1	450.55	4.98	5.80	0.23	0.21	4EIY
62	2.15 ± 0.20	0.38 ± 0.04	5.66	386.46	5.67	4.54	0.31	0.23	4EIY

[a]Displacement of [^{3}H]ZM 241385 binding at the human A_{2A} or A_1 AR expressed in HEK293 cells. Data are expressed as geometric mean values of at least two runs ± standard error of the mean (SEM). [b]Molecular weight. [c]Predicted octanol/water partition coefficient. [d]Ligand efficiency, defined as LE = 1.37pK_i/heavy atom. [e]Pairwise similarity based on the FCFP_4 fingerprints for each identified antagonist with the known antagonists of the A_{2A} AR. [f]Crystal complex structure of the A_{2A} AR used in the *Glide* docking. [g]Not determined.

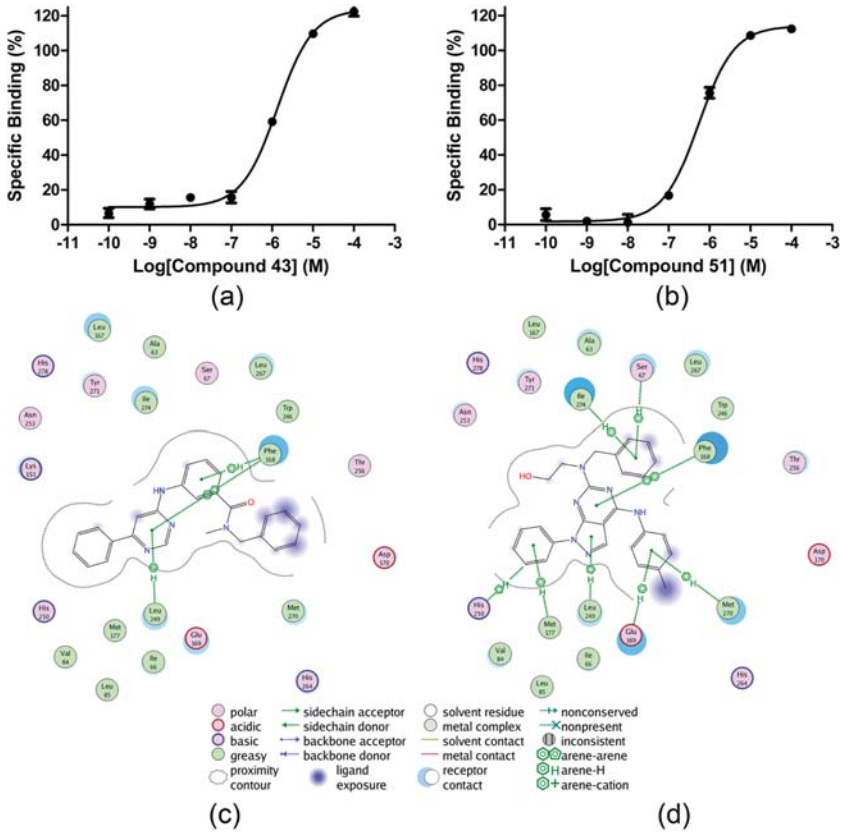

Figure 4. (a, b) Radioligand competition binding curves for compounds (a) **43** and (b) **51** against the A_{2A} AR. (c, d) Schematic representations of the predicted interactions derived from *Glide* docking between the A_{2A} AR and compounds (c) **43** and (d) **51**.

cAMP Functional Assays for the Identified A_{2A} AR Antagonists. Compounds **43** and **51** are the most potent compounds, with K_i values below 1 μM. In order to confirm that compounds **43** and **51** are functional antagonists, they were profiled in a cell-based cAMP assay. Preladelant was used as the control compound (IC_{50} = 3.1 nM). The potential antagonist activities of the two compounds against the A_{2A} AR were assessed over a full range of concentrations. Both **43** and **51** induced significant suppression of the A_{2A} AR, as indicated by the cAMP−compound concentration curves (Figure 6). Compounds **43** and **51** inhibited cAMP production (IC_{50} = 1.67 μM and 1.80 μM, respectively), suggesting that both of them are functional antagonists of the A_{2A} AR.

Haloperidol-Induced Catalepsy Rat Models. The HIC rat model for PD was then employed to evaluate the in vivo activities of compounds **43** and **51**. Preladenant (3, 10, and 30 mg/kg i.p.) was used as the positive control. The results for compounds **43** and **51** are presented in Figure 7. Both

DOI: 10.1021/acs.jcim.7b00188
J. Chem. Inf. Model. 2017, 57, 1474−1487

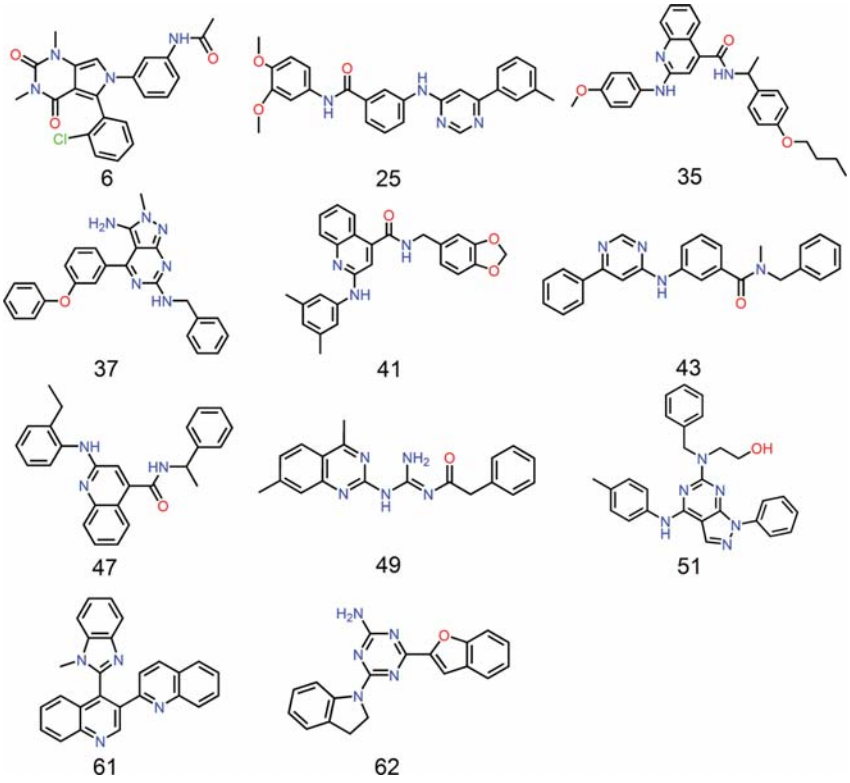

Figure 5. Chemical structures of the 11 identified A_{2A} AR antagonists using comparative-docking-based VS.

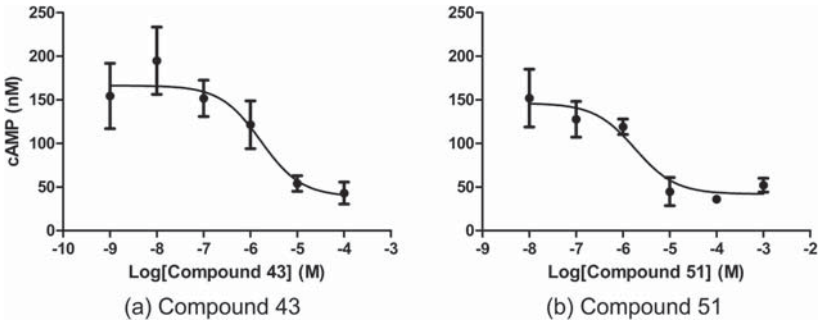

Figure 6. Levels of intracellular cAMP production at compound concentrations of 100 μM to 1 nM for compounds (a) **43** and (b) **51**.

43 and **51** demonstrated significant reversal of HIC at a dose of 30 mg/kg. There was no significant effect at doses of 3 and 10 mg/kg, indicating that a minimum effective dose was reached at 30 mg/kg, probably reflecting the suboptimal A_{2A} AR antagonist activities of these two compounds. Nevertheless, our preliminary study proved that compounds **43** and **51** had potential anti-PD effects in the HIC rat model.

Lead Optimization Based on Substructure Searching. On the basis of the scaffolds of compounds **43** and **51**, substructure searching was conducted to screen the ChemDiv database, and 12 analogues of compound **43** (Table 3) and 20 analogues of compound **51** (Table 4) were identified and purchased for bioassays. The 32 analogues of the two identified A_{2A} AR antagonists were subjected to a radioligand competition binding assay using stably transfected A_{2A}R-HEK293 cell membranes with [^{3}H]ZM241385 at a final concentration of 0.1 nM to detect specific binding. According to the results shown in Tables 3 and 4, two analogues of compound **43** (compounds **70** and **71**) and six analogues of compound **51** (compounds **79**, **80**, **82**, **84**, **86**, and **87**) had percent inhibition over 85% in the initial test. The further binding affinity assays of the eight identified analogues were conducted. The two analogues of

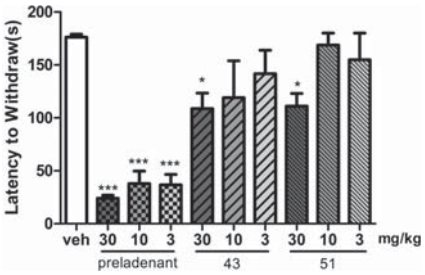

Figure 7. Effects of compounds **43** and **51** in the HIC bar test. Mean descent latency (±standard error) in seconds is shown. The vehicle bar represents the mean and standard error from four experiments. *, $p < 0.05$ and ***, $p < 0.001$ vs vehicle controls.

DOI: 10.1021/acs.jcim.7b00188
J. Chem. Inf. Model. 2017, 57, 1474−1487

Table 3. Binding Affinities and Chemical Structures for the 12 Analogues of Compound 43

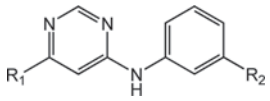

Compd	R_1	R_2	I (%)[a]	A_{2A} K_i (μM) ± SEM[b]	MW[c]	log$P$[d]
43		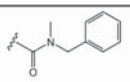	114.44	0.42 ± 0.04	425.49	6.38
64		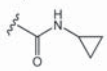	27.20	ND[e]	330.39	3.79
65			33.63	ND	332.41	4.02
66			52.24	ND	344.42	3.96
67			2.77	ND	350.40	4.23
68		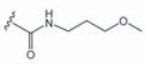	49.41	ND	362.43	3.23
69		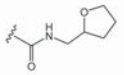	37.02	ND	374.44	2.69
70		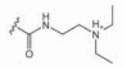	90.48	6.99±0.08	390.51	4.13
71		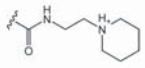	89.76	4.48±0.55	402.52	4.35
72		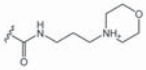	67.21	ND	418.52	2.37
73		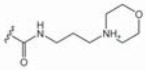	59.29	ND	436.51	3.39
74		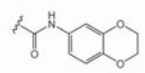	7.19	ND	442.45	4.86
75		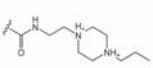	70.81	ND	464.59	4.47

[a]Homologous screening was performed using membranes of mammalian cells overexpressing the A_{2A} AR with a compound concentration of 100 μM. [b]Displacement of [^{3}H]ZM241385 binding at the human A_{2A} AR expressed in HEK293 cells. Data are expressed as geometric mean values of at least two runs ± SEM. [c]Molecular weight. [d]Predicted octanol/water partition coefficient. [e]Not determined.

compound **43** did not have improved binding affinities toward the A_{2A} AR (K_i values below 10 μM) compared with the parent compound **43**. Encouragingly, five out of the six analogues of compound **51** showed better A_{2A} AR binding affinities than compound **51** (A_{2A} K_i < 0.25 μM). Among them, two most potent compounds (compounds **79** and **84**) have affinities for the A_{2A} AR of 0.048 and 0.054 μM, respectively (Table 4). Besides, compounds **79** and **84** also have satisfactory physicochemical properties and optimal ligand efficiencies[54] (better than 0.36 kcal/mol per heavy atom; Table 4). The interaction pattern between compound **84** and the A_{2A} AR in the predicted binding pose and the radioligand competition

Table 4. Binding Affinities and Chemical Structures for the 20 Analogues of Compound 51

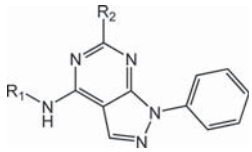

Compd	R_1	R_2	I (%)[a]	K_i (μM) ± SEM[b]			MW[c]	log$P$[d]
				A_{2A}	A_1	A_{2A}-A_1		
51			116.12	0.27 ± 0.06	ND[e]	ND	333.39	6.57
76			83.13	ND	ND	ND	330.40	4.16
77			73.40	ND	ND	ND	346.39	3.66
78			79.62	ND	ND	ND	346.39	3.66
79			102.68	0.048 ± 0.009	0.31 ± 0.035	0.15	360.42	3.62
80			97.07	3.10 ± 0.14	ND	ND	360.42	3.62
81			2.79	ND	ND	ND	360.42	4.29
82			100.11	0.22 ± 0.03	0.16 ± 0.005	1.4	364.38	3.34
83			80.31	ND	ND	ND	374.45	4.26
84			101.49	0.054 ± 0.003	ND	< 0.1	374.45	3.69
85			82.36	ND	ND	ND	374.45	4.00
86			102.58	0.19 ± 0.02	0.47 ± 0.067	0.4	376.42	3.12
87			97.58	0.17 ± 0.01	ND	< 0.1	374.45	4.12
88			42.68	ND	ND	ND	386.46	4.75
89			50.66	ND	ND	ND	390.42	4.20
90			72.19	ND	ND	ND	404.47	3.85
91			46.62	ND	ND	ND	416.51	3.73
92			17.78	ND	ND	ND	416.49	4.33
93			53.15	ND	ND	ND	416.51	3.50
94			9.07	ND	ND	ND	416.51	4.25
95			55.50	ND	ND	ND	416.51	4.25

[a]Homologous screening was performed using membranes of mammalian cells overexpressing the A_{2A} AR with a compound concentration of 100 μM. [b]Displacement of [^{3}H]ZM241385 binding at the human A_{2A} A_1 AR expressed in HEK293 cells. Data are expressed as geometric

DOI: 10.1021/acs.jcim.7b00188
J. Chem. Inf. Model. 2017, 57, 1474−1487

Table 4. continued

mean values of at least two runs ± SEM. [c]Molecular weight. [d]Predicted octanol/water partition coefficient. [e]Not determined.

binding curve for compound **84** are illustrated in Figure 8a and Figure 8b, respectively.

The five analogues of compound **51** that showed improved binding affinities toward the A_{2A} AR (compounds **79**, **82**, **84**, **86**, and **87**) were subjected to the A_{2A}/A_1 selectivity testing (Table 4). We found that two compounds (**84** and **87**) exhibited high selectivity for the A_{2A} AR (A_{2A}/A_1 fold < 0.1). Furthermore, the most promising analogue, compound **84**, was profiled in the cell-based cAMP assay. As shown in Figure 8c, compound **84** induced significant suppression of cAMP (IC_{50} = 0.3 μM), suggesting that it is a functional antagonist of the A_{2A} AR. Finally, the HIC rat model was also applied to validate the potential anti-PD efficacy of compound **84.** As shown in Figure 8d, compound **84** demonstrated significant reversal of HIC at all three tested doses (3, 10, 30 mg/kg) and exhibited better efficacy than its parent compound.

In order to understand the differences in the antagonist activities among compound **51** and the five promising analogues of compound **51** (compounds **79**, **82**, **84**, **86**, and **87**), the binding patterns predicted by *Glide* docking for the six compounds were compared (Figure 9) and the interaction spectra between the key residues and those compounds were analyzed using MM/GBSA free energy calculations and decompositions (Figure 10; detailed information on the calculations can be found in the Supporting Information).[32,33,55−62] First, the six ligands of the A_{2A} AR were docked into the crystal complex of the A_{2A} AR with the best discrimination power for VS (PDB ID 4EIY) using the XP scoring function of *Glide*. The results demonstrated that the predictions from *Glide* docking can rank the binding affinities of the six antagonists of the A_{2A} AR efficiently, as indicated by the high correlation coefficient between the docking scores and experimental antagonist activities (r^2 = 0.905). The MM/GBSA free energy decomposition analysis was utilized to discern the contribution of each residue to antagonist binding. As shown in Figure 10b,d), the two most promising A_{2A} AR antagonists (compounds **79** and **84**) share similar interaction patterns with the residues in the binding pocket of the A_{2A} AR. For compound **79**, the residues Ala59, Val84, Pro168, Leu283, Asn253, and Ile274 serve as the key residues for the binding, and their contributions to the binding (ΔG_{pred}) are all lower than −1.5 kcal/mol. Compared with compound **79**, compound **84** has similar key binding residues (Val84, Pro168, Leu249, Asn253, and Ile274) and the only difference is Ile80 (−1.81 kcal/mol) instead of Ala59 (−0.08 kcal/mol). A similar phenomenon can also be observed for the other four compounds (compounds **51**, **82**, **86**, and **87**). According to the residue−antagonist interaction spectra of the dominant amino acids for the six antagonists depicted in Figure 10, we can see that residues Ala61, Val84, Pro168, Leu249, Asn253, and Ile274 play a very important role in achieving promising antagonist activity against the A_{2A} AR. For example, the core structure of the six investigated antagonists, 1*H*-pyrazolo[3,4-*d*]pyrimidine, can form hydrogen-bonding interactions with Asn253 and $\pi-\pi$ stacking interactions with residues Phe168 and Ieu249. The other residues around the binding pocket of the A_{2A} AR, such as Ala63 and Ile80, also have positive contributions. This finding may guide us to design more optimal A_{2A} AR antagonists in the future.

CONCLUSIONS

In the current work, we compared the performances of the *Glide*-docking-based VS based on different A_{2A} AR complex crystal structures and identified two crystal templates with the

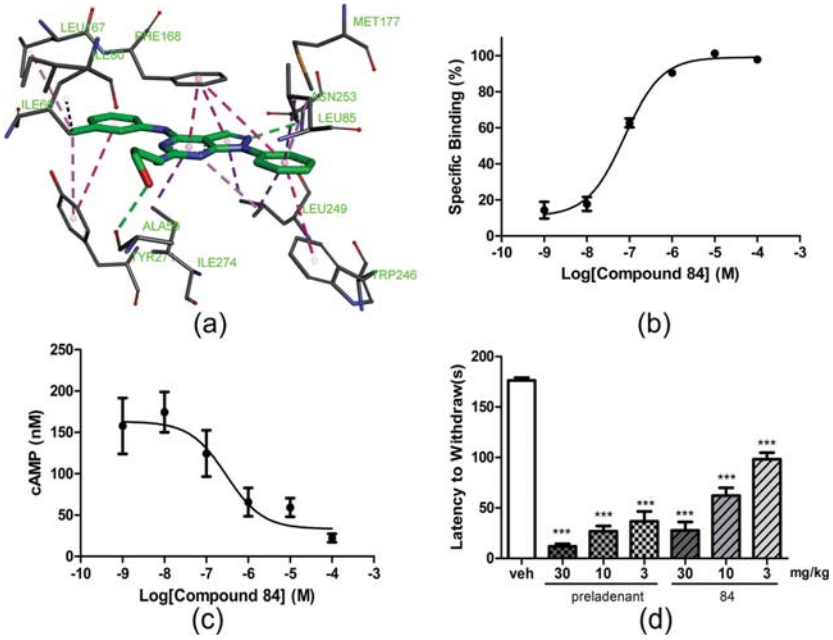

Figure 8. (a) Interactions between compound **84** and A_{2A} AR in the predicted pose. (b) Radioligand competition binding curve of compound **84**. (c) Levels of intracellular cAMP production at compound concentrations of 100 μM to 1 nM for compound **84**. (d) Effect of compound **84** in the HIC bar test. Mean descent latency (±standard error) in seconds is shown. The vehicle bar represents the mean and standard error from four experiments. *, $p < 0.05$ and ***, $p < 0.001$ vs vehicle controls.

DOI: 10.1021/acs.jcim.7b00188
J. Chem. Inf. Model. 2017, 57, 1474−1487

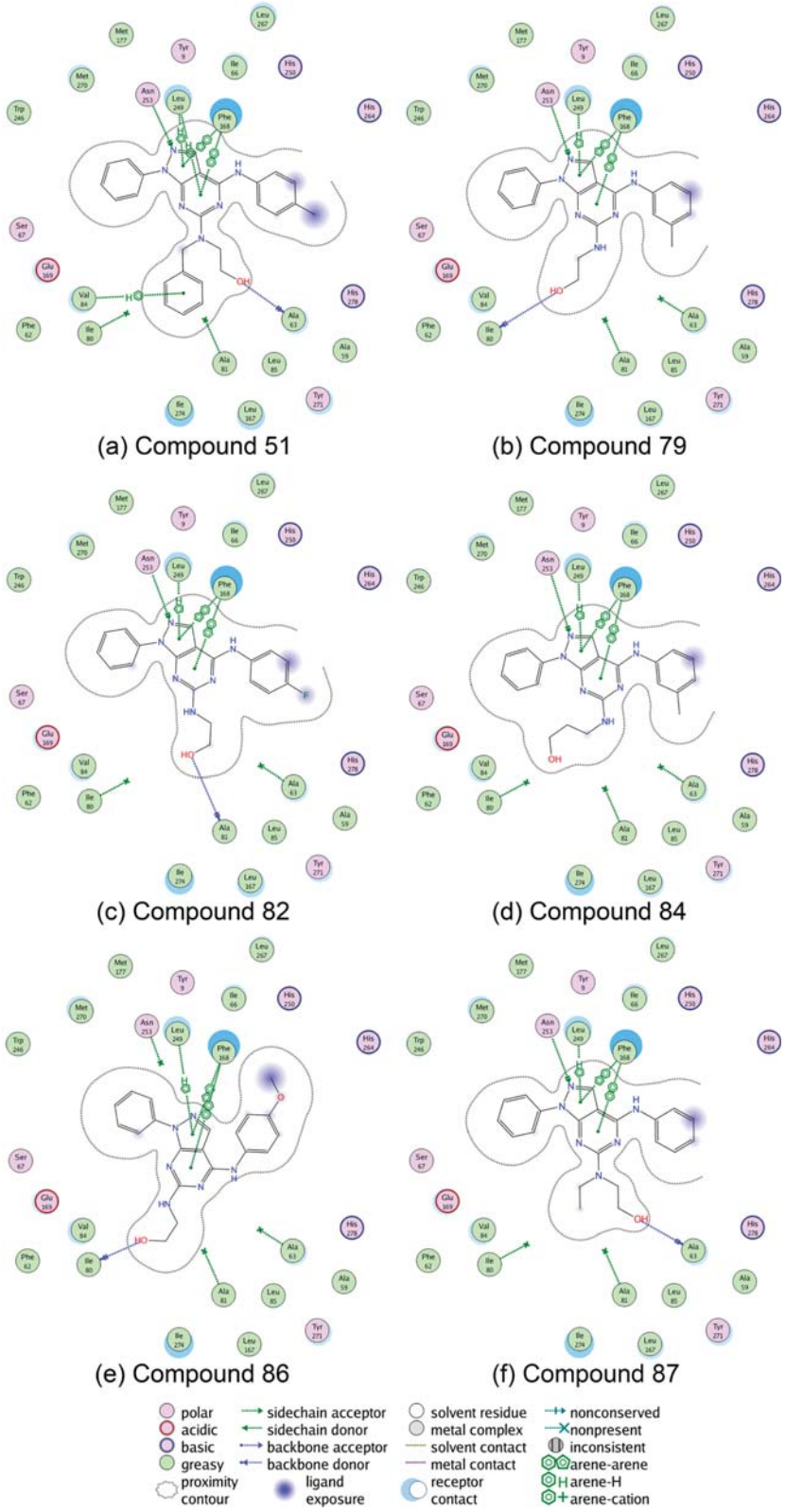

Figure 9. 2D schematic diagrams of the binding patterns predicted using the XP scoring function for *Glide* docking of compounds (a) **51**, (b) **79**, (c) **82**, (d) **84**, (e) **86**, and (f) **87**.

most reliable prediction capacity in docking-based VS. A total of 63 potential hits predicted by the docking-based VS were submitted to bioassays, and 11 of them exhibited substantial activity against the A_{2A} AR, including two compounds (**43** and **51**)

DOI: 10.1021/acs.jcim.7b00188
J. Chem. Inf. Model. 2017, 57, 1474−1487

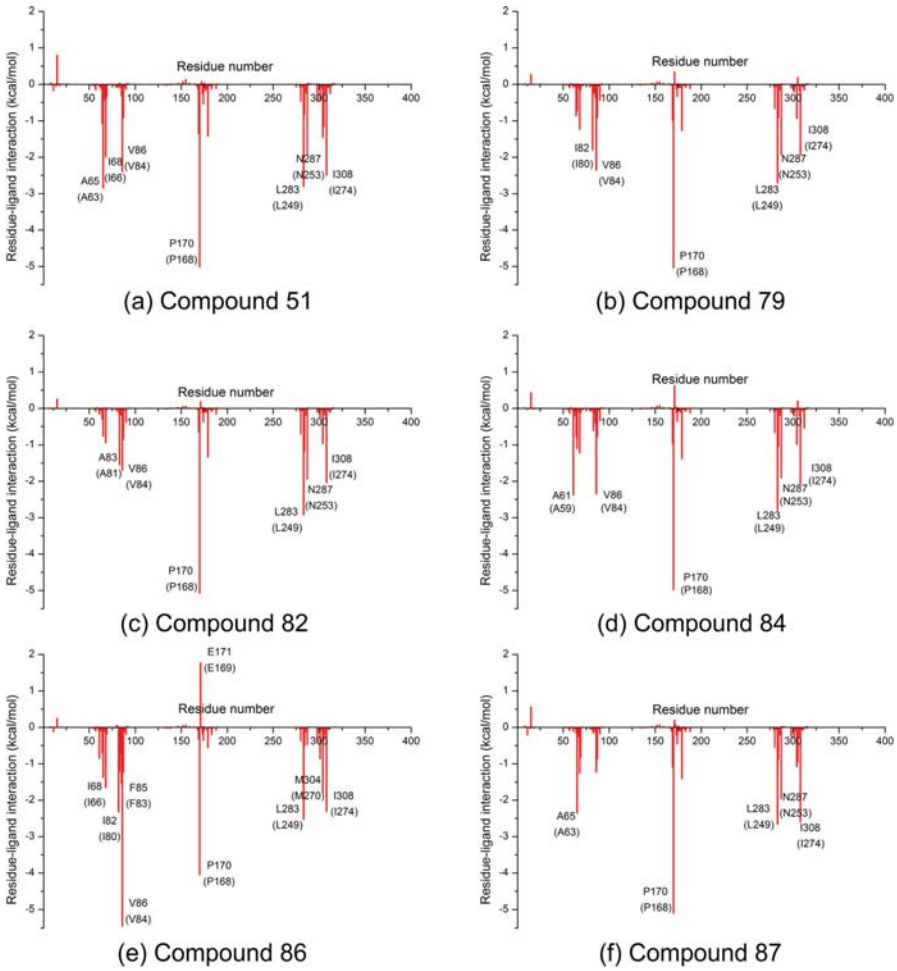

Figure 10. Contributions of the important residues to the binding of compounds (a) **51**, (b) **79**, (c) **82**, (d) **84**, (e) **86**, and (f) **87** to the A_{2A} AR. All of the structures are average conformations generated from the last 3 ns of the molecular dynamics trajectories. The average energetic contributions of the dominant residues from the MM/GBSA decomposition analysis are also plotted.

with A_{2A} AR K_i values below 1 μM. The two compounds were confirmed as functional A_{2A} AR antagonists with good selectivity for the A_{2A} AR. Further optimization based on the core structural scaffolds of compounds **43** and **51** led to the discovery of compound **84** as an excellent A_{2A} AR antagonist. Compound **84** exhibits an A_{2A} affinity under 60 nM, good A_{2A}/A_1 selectivity, and improved efficacy in the HIC model.

■ ASSOCIATED CONTENT

Supporting Information

The Supporting Information is available free of charge on the ACS Publications website at DOI: 10.1021/acs.jcim.7b00188.

Binding affinities of the A_{2A} AR for the tested compounds at a concentration of 100 μM (Table S1) and protocols for the molecular dynamics simulations and MM/GBSA binding free energy calculations and decompositions (PDF)

■ AUTHOR INFORMATION

Corresponding Authors

*E-mail: tingjunhou@zju.edu.cn or tingjunhou@hotmail.com.
*E-mail: zhenxuechu@suda.edu.cn.

ORCID

Youyong Li: 0000-0002-5248-2756
Tingjun Hou: 0000-0001-7227-2580

Author Contributions

‖S.T., X.W., and L.L. contributed equally.

Notes

The authors declare no competing financial interest.

■ ACKNOWLEDGMENTS

This study was supported by the National Natural Science Foundation of China (81502982, 81130023, 81371278, 81273372, and 81473090), the National Major Basic Research Program of China (2016YFA0501701 and 2016YFB0201700), the National Basic Research Plan (973) of the Ministry of Science and Technology of China (2011CB504403), the Specialized Research Fund for the Doctoral Program of Higher Education of China (20133201110017), the China Postdoctoral Science Foundation (2015T80586 and 2015M581862), the Priority Academic Program Development of the Jiangsu Higher Education Institutes (PAPD), and the Jiangsu Key Laboratory of Translational Research for Neuropsychiatric Diseases (BM2013003).

DOI: 10.1021/acs.jcim.7b00188
J. Chem. Inf. Model. 2017, 57, 1474−1487

REFERENCES

(1) Hattori, N. Movement disorders: advances in 2015. *Lancet Neurol.* **2016**, *15*, 8−9.

(2) Zhang, A.; Neumeyer, J. L.; Baldessarini, R. J. Recent progress in development of dopamine receptor subtype-selective agents: Potential therapeutics for neurological and psychiatric disorders. *Chem. Rev.* **2007**, *107*, 274−302.

(3) Ye, N.; Neumeyer, J. L.; Baldessarini, R. J.; Zhen, X.; Zhang, A. Update 1 of: Recent progress in development of dopamine receptor subtype-selective agents: Potential therapeutics for neurological and psychiatric disorders. *Chem. Rev.* **2013**, *113*, PR123−PR178.

(4) Bastide, M. F.; Meissner, W. G.; Picconi, B.; Fasano, S.; Fernagut, P. O.; Feyder, M.; Francardo, V.; Alcacer, C.; Ding, Y. M.; Brambilla, R.; Fisone, G.; Stoessl, A. J.; Bourdenx, M.; Engeln, M.; Navailles, S.; De Deurwaerdere, P.; Ko, W. K. D.; Simola, N.; Morelli, M.; Groc, L.; Rodriguez, M. C.; Gurevich, E. V.; Quik, M.; Morari, M.; Mellone, M.; Gardoni, F.; Tronci, E.; Guehl, D.; Tison, F.; Crossman, A. R.; Kang, U. J.; Steece-Collier, K.; Fox, S.; Carta, M.; Cenci, M. A.; Bezard, E. Pathophysiology of L-dopa-induced motor and non-motor complications in Parkinson's disease. *Prog. Neurobiol.* **2015**, *132*, 96−168.

(5) Mo, J.; Zhang, H.; Yu, L. P.; Sun, P. H.; Jin, G. Z.; Zhen, X. C. L-Stepholidine reduced L-DOPA-induced dyskinesia in 6-OHDA-lesioned rat model of Parkinson's disease. *Neurobiol. Aging* **2010**, *31*, 926−936.

(6) Antonini, A.; Cilia, R. Behavioural adverse effects of dopaminergic treatments in Parkinson's disease Incidence, neurobiological basis, management and prevention. *Drug Saf.* **2009**, *32*, 475−488.

(7) Bonuccelli, U.; Del Dotto, P. New pharmacologic horizons in the treatment of Parkinson disease. *Neurology* **2006**, *67*, S30−S38.

(8) Ruiz, M. d. L.; Lim, Y.-H.; Zheng, J. Adenosine A_{2A} receptor as a drug discovery target. *J. Med. Chem.* **2014**, *57*, 3623−3650.

(9) Shook, B. C.; Jackson, P. F. Adenosine A2A receptor antagonists and Parkinson's disease. *ACS Chem. Neurosci.* **2011**, *2*, 555−567.

(10) Salamone, J. D. Facing dyskinesia in Parkinson's disease: nondopaminergic approaches. *Drugs Future* **2010**, *35*, 567−573.

(11) Schwarzschild, M. A.; Agnati, L.; Fuxe, K.; Chen, J.-F.; Morelli, M. Targeting adenosine A_{2A} receptors in Parkinson's disease. *Trends Neurosci.* **2006**, *29*, 647−654.

(12) Lozano, A. M.; Lang, A. E.; Hutchison, W. D.; Dostrovsky, J. O. New developments in understanding the etiology of Parkinson's disease and in its treatment. *Curr. Opin. Neurobiol.* **1998**, *8*, 783−790.

(13) Pollack, A.; Fink, J. Adenosine antagonists potentiate D2 dopamine-dependent activation of Fos in the striatopallidal pathway. *Neuroscience* **1995**, *68*, 721−728.

(14) Fredduzzi, S.; Moratalla, R.; Monopoli, A.; Cuellar, B.; Xu, K.; Ongini, E.; Impagnatiello, F.; Schwarzschild, M. A.; Chen, J.-F. Persistent behavioral sensitization to chronic L-DOPA requires A_{2A} adenosine receptors. *J. Neurosci.* **2002**, *22*, 1054−1062.

(15) Pinna, A. Novel investigational adenosine A_{2A} receptor antagonists for Parkinson's disease. *Expert Opin. Invest. Drugs* **2009**, *18*, 1619−1631.

(16) Zheng, J.; Yang, Z.; Li, X.; Li, L.; Ma, H.; Wang, M.; Zhang, H.; Zhen, X.; Zhang, X. Optimization of 6-Heterocyclic-2-(1H-pyrazol-1-yl)-N-(pyridin-2-yl)pyrimidin-4-amine as potent adenosine A_{2A} receptor antagonists for the treatment of Parkinson's disease. *ACS Chem. Neurosci.* **2014**, *5*, 674−682.

(17) Zhang, X.; Tellew, J. E.; Luo, Z.; Moorjani, M.; Lin, E.; Lanier, M. C.; Chen, Y.; Williams, J. P.; Saunders, J.; Lechner, S. M.; Markison, S.; Joswig, T.; Petroski, R.; Piercey, J.; Kargo, W.; Malany, S.; Santos, M.; Gross, R. S.; Wen, J.; Jalali, K.; O'Brien, Z.; Stotz, C. E.; Crespo, M. I.; Diaz, J.-L.; Slee, D. H. Lead optimization of 4-acetylamino-2-(3,5-dimethylpyrazol-1-yl)-6-pyridylpyrimidines as A_{2A} adenosine receptor antagonists for the treatment of Parkinson's disease. *J. Med. Chem.* **2008**, *51*, 7099−7110.

(18) Yang, Z.; Li, X.; Ma, H.; Zheng, J.; Zhen, X.; Zhang, X. Replacement of amide with bioisosteres led to a new series of potent adenosine A_{2A} receptor antagonists. *Bioorg. Med. Chem. Lett.* **2014**, *24*, 152−155.

(19) Zhang, X.; Rueter, J. K.; Chen, Y.; Moorjani, M.; Lanier, M. C.; Lin, E.; Gross, R. S.; Tellew, J. E.; Williams, J. P.; Lechner, S. M.; Markison, S.; Joswig, T.; Malany, S.; Santos, M.; Castro-Palomino, J. C.; Crespo, M. I.; Prat, M.; Gual, S.; Diaz, J.-L.; Saunders, J.; Slee, D. H. Synthesis of N-pyrimidinyl-2-phenoxyacetamides as adenosine A_{2A} receptor antagonists. *Bioorg. Med. Chem. Lett.* **2008**, *18*, 1778−1783.

(20) Bajorath, J. Integration of virtual and high-throughput screening. *Nat. Rev. Drug Discovery* **2002**, *1*, 882−94.

(21) Hou, T. J.; Xu, X. J. Recent development and application of virtual screening in drug discovery: an overview. *Curr. Pharm. Des.* **2004**, *10*, 1011−1033.

(22) Kitchen, D. B.; Decornez, H.; Furr, J. R.; Bajorath, J. Docking and scoring in virtual screening for drug discovery: Methods and applications. *Nat. Rev. Drug Discovery* **2004**, *3*, 935−949.

(23) Shoichet, B. K.; McGovern, S. L.; Wei, B. Q.; Irwin, J. J. Lead discovery using molecular docking. *Curr. Opin. Chem. Biol.* **2002**, *6*, 439−446.

(24) Xu, L.; Zhang, Y.; Zheng, L.; Qiao, C.; Li, Y.; Li, D.; Zhen, X.; Hou, T. Discovery of Novel Inhibitors Targeting the Macrophage Migration Inhibitory Factor via Structure-Based Virtual Screening and Bioassays. *J. Med. Chem.* **2014**, *57*, 3737−3745.

(25) Carlsson, J.; Yoo, L.; Gao, Z.-G.; Irwin, J. J.; Shoichet, B. K.; Jacobson, K. A. Structure-based discovery of A_{2A} adenosine receptor ligands. *J. Med. Chem.* **2010**, *53*, 3748−3755.

(26) Katritch, V.; Jaakola, V.-P.; Lane, J. R.; Lin, J.; Ijzerman, A. P.; Yeager, M.; Kufareva, I.; Stevens, R. C.; Abagyan, R. Structure-based discovery of novel chemotypes for adenosine A_{2A} receptor antagonists. *J. Med. Chem.* **2010**, *53*, 1799−1809.

(27) Congreve, M.; Andrews, S. P.; Dore, A. S.; Hollenstein, K.; Hurrell, E.; Langmead, C. J.; Mason, J. S.; Ng, I. W.; Tehan, B.; Zhukov, A.; Weir, M.; Marshall, F. H. Discovery of 1,2,4-triazine derivatives as adenosine A_{2A} antagonists using structure based drug design. *J. Med. Chem.* **2012**, *55*, 1898−1903.

(28) Langmead, C. J.; Andrews, S. P.; Congreve, M.; Errey, J. C.; Hurrell, E.; Marshall, F. H.; Mason, J. S.; Richardson, C. M.; Robertson, N.; Zhukov, A.; Weir, M. Identification of novel adenosine A_{2A} receptor antagonists by virtual screening. *J. Med. Chem.* **2012**, *55*, 1904−1909.

(29) Zhukov, A.; Andrews, S. P.; Errey, J. C.; Robertson, N.; Tehan, B.; Mason, J. S.; Marshall, F. H.; Weir, M.; Congreve, M. Biophysical mapping of the adenosine A_{2A} receptor. *J. Med. Chem.* **2011**, *54*, 4312−4323.

(30) Rodriguez, D.; Gao, Z.-G.; Moss, S. M.; Jacobson, K. A.; Carlsson, J. Molecular docking screening using agonist-bound GPCR structures: Probing the A_{2A} adenosine receptor. *J. Chem. Inf. Model.* **2015**, *55*, 550−563.

(31) Jaakola, V.-P.; Griffith, M. T.; Hanson, M. A.; Cherezov, V.; Chien, E. Y. T.; Lane, J. R.; Ijzerman, A. P.; Stevens, R. C. The 2.6 angstrom crystal structure of a human A_{2A} adenosine receptor bound to an antagonist. *Science* **2008**, *322*, 1211−1217.

(32) Pan, P.; Tian, S.; Sun, H.; Kong, X.; Zhou, W.; Li, D.; Li, Y.; Hou, T. Identification and preliminary SAR analysis of novel type-I inhibitors of TIE-2 via structure-based virtual screening and biological evaluation in in vitro models. *J. Chem. Inf. Model.* **2015**, *55*, 2693−2704.

(33) Shen, M.; Tian, S.; Pan, P.; Sun, H.; Li, D.; Li, Y.; Zhou, H.; Li, C.; Lee, S. M.-Y.; Hou, T. Discovery of novel ROCK1 inhibitors via integrated virtual screening strategy and bioassays. *Sci. Rep.* **2015**, *5*, 16749.

(34) Tian, S.; Sun, H.; Pan, P.; Li, D.; Zhen, X.; Li, Y.; Hou, T. Assessing an ensemble docking-based virtual screening strategy for kinase targets by considering protein flexibility. *J. Chem. Inf. Model.* **2014**, *54*, 2664−2679.

(35) Tian, S.; Sun, H.; Li, Y.; Pan, P.; Li, D.; Hou, T. Development and evaluation of an integrated virtual screening strategy by combining molecular docking and pharmacophore searching based on multiple protein structures. *J. Chem. Inf. Model.* **2013**, *53*, 2743−2756.

(36) Cozzini, P.; Kellogg, G. E.; Spyrakis, F.; Abraham, D. J.; Costantino, G.; Emerson, A.; Fanelli, F.; Gohlke, H.; Kuhn, L. A.;

DOI: 10.1021/acs.jcim.7b00188
J. Chem. Inf. Model. 2017, 57, 1474−1487

Morris, G. M.; Orozco, M.; Pertinhez, T. A.; Rizzi, M.; Sotriffer, C. A. Target flexibility: an emerging consideration in drug discovery and design. *J. Med. Chem.* **2008**, *51*, 6237−6255.
(37) B-Rao, C.; Subramanian, J.; Sharma, S. D. Managing protein flexibility in docking and its applications. *Drug Discovery Today* **2009**, *14*, 394−400.
(38) Zhou, S.; Li, Y.; Hou, T. Feasibility of using molecular docking-based virtual screening for searching dual target kinase inhibitors. *J. Chem. Inf. Model.* **2013**, *53*, 982−996.
(39) Berman, H. M.; Westbrook, J.; Feng, Z.; Gilliland, G.; Bhat, T. N.; Weissig, H.; Shindyalov, I. N.; Bourne, P. E. The Protein Data Bank. *Nucleic Acids Res.* **2000**, *28*, 235−242.
(40) Dore, A. S.; Robertson, N.; Errey, J. C.; Ng, I.; Hollenstein, K.; Tehan, B.; Hurrell, E.; Bennett, K.; Congreve, M.; Magnani, F.; Tate, C. G.; Weir, M.; Marshall, F. H. Structure of the adenosine A_{2A} receptor in complex with ZM241385 and the xanthines XAC and caffeine. *Structure* **2011**, *19*, 1283−1293.
(41) Hino, T.; Arakawa, T.; Iwanari, H.; Yurugi-Kobayashi, T.; Ikeda-Suno, C.; Nakada-Nakura, Y.; Kusano-Arai, O.; Weyand, S.; Shimamura, T.; Nomura, N.; Cameron, A. D.; Kobayashi, T.; Hamakubo, T.; Iwata, S.; Murata, T. G-protein-coupled receptor inactivation by an allosteric inverse-agonist antibody. *Nature* **2012**, *482*, 237−240.
(42) Liu, W.; Chun, E.; Thompson, A. A.; Chubukov, P.; Xu, F.; Katritch, V.; Han, G. W.; Roth, C. B.; Heitman, L. H.; Ijzerman, A. P.; Cherezov, V.; Stevens, R. C. Structural basis for allosteric regulation of GPCRs by sodium ions. *Science* **2012**, *337*, 232−236.
(43) Tian, S.; Li, Y.; Li, D.; Xu, X.; Wang, J.; Zhang, Q.; Hou, T. Modeling compound-target interaction network of traditional Chinese medicines for type II diabetes mellitus: Insight for polypharmacology and drug design. *J. Chem. Inf. Model.* **2013**, *53*, 1787−1803.
(44) Gatica, E. A.; Cavasotto, C. N. Ligand and decoy sets for docking to G protein-coupled receptors. *J. Chem. Inf. Model.* **2012**, *52*, 1−6.
(45) Irwin, J. J.; Shoichet, B. K. ZINC - A free database of commercially available compounds for virtual screening. *J. Chem. Inf. Model.* **2005**, *45*, 177−182.
(46) Krüger, D. M.; Evers, A. Comparison of structure- and ligand-based virtual screening protocols considering hit list complementarity and enrichment factors. *ChemMedChem* **2010**, *5*, 148−158.
(47) Lipinski, C. A.; Lombardo, F.; Dominy, B. W.; Feeney, P. J. Experimental and computational approaches to estimate solubility and permeability in drug discovery and development settings. *Adv. Drug Delivery Rev.* **2001**, *46*, 3−26.
(48) Tian, S.; Wang, J.; Li, Y.; Xu, X.; Hou, T. Drug-likeness analysis of traditional Chinese medicines: Prediction of drug-likeness using machine learning approaches. *Mol. Pharmaceutics* **2012**, *9*, 2875−2886.
(49) Tian, S.; Wang, J.; Li, Y.; Li, D.; Xu, L.; Hou, T. The application of in silico drug-likeness predictions in pharmaceutical research. *Adv. Drug Delivery Rev.* **2015**, *86*, 2−10.
(50) Walters, W. P.; Stahl, M. T.; Murcko, M. A. Virtual screening - an overview. *Drug Discovery Today* **1998**, *3*, 160−178.
(51) Yang, Z.; Li, L.; Zheng, J.; Ma, H.; Tian, S.; Li, J.; Zhang, H.; Zhen, X.; Zhang, X. Identification of a new series of potent adenosine A2A receptor antagonists based on 4-amino-5-carbonitrile pyrimidine template for the treatment of Parkinson's disease. *ACS Chem. Neurosci.* **2016**, *7*, 1575−1584.
(52) Bemis, G. W.; Murcko, M. A. The properties of known drugs 0.1. Molecular frameworks. *J. Med. Chem.* **1996**, *39*, 2887−2893.
(53) Liu, T.; Lin, Y.; Wen, X.; Jorissen, R. N.; Gilson, M. K. BindingDB: a web-accessible database of experimentally determined protein-ligand binding affinities. *Nucleic Acids Res.* **2007**, *35*, D198−D201.
(54) Hopkins, A. L.; Groom, C. R.; Alex, A. Ligand efficiency: a useful metric for lead selection. *Drug Discovery Today* **2004**, *9*, 430−431.
(55) Sun, H.; Li, Y.; Shen, M.; Tian, S.; Xu, L.; Pan, P.; Guan, Y.; Hou, T. Assessing the performance of MM/PBSA and MM/GBSA methods. 5. Improved docking performance using high solute dielectric constant MM/GBSA and MM/PBSA rescoring. *Phys. Chem. Chem. Phys.* **2014**, *16*, 22035−22045.
(56) Xu, L.; Sun, H.; Li, Y.; Wang, J.; Hou, T. Assessing the performance of MM/PBSA and MM/GBSA methods. 3. The impact of force fields and ligand charge models. *J. Phys. Chem. B* **2013**, *117*, 8408−8421.
(57) Hou, T.; Wang, J.; Li, Y.; Wang, W. Assessing the performance of the MM/PBSA and MM/GBSA methods. 1. The accuracy of binding free energy calculations based on molecular dynamics simulations. *J. Chem. Inf. Model.* **2011**, *51*, 69−82.
(58) Hou, T.; Wang, J.; Li, Y.; Wang, W. Assessing the performance of the molecular mechanics/poisson boltzmann surface area and molecular mechanics/generalized born surface area methods. II. The accuracy of ranking poses generated from docking. *J. Comput. Chem.* **2011**, *32*, 866−877.
(59) Chen, F.; Liu, H.; Sun, H.; Pan, P.; Li, Y.; Li, D.; Hou, T. Assessing the performance of the MM/PBSA and MM/GBSA methods. 6. Capability to predict protein-protein binding free energies and re-rank binding poses generated by protein-protein docking. *Phys. Chem. Chem. Phys.* **2016**, *18*, 22129−22139.
(60) Hou, T.; Li, N.; Li, Y.; Wang, W. Characterization of Domain-Peptide Interaction Interface: Prediction of SH3 Domain-Mediated Protein-Protein Interaction Network in Yeast by Generic Structure-Based Models. *J. Proteome Res.* **2012**, *11*, 2982−2995.
(61) Sun, H.; Li, Y.; Tian, S.; Xu, L.; Hou, T. Assessing the performance of MM/PBSA and MM/GBSA methods. 4. Accuracies of MM/PBSA and MM/GBSA methodologies evaluated by various simulation protocols using PDBbind data set. *Phys. Chem. Chem. Phys.* **2014**, *16*, 16719−16729.
(62) Sun, H.; Tian, S.; Zhou, S.; Li, Y.; Li, D.; Xu, L.; Shen, M.; Pan, P.; Hou, T. Revealing the favorable dissociation pathway of type II kinase inhibitors via enhanced sampling simulations and two-end-state calculations. *Sci. Rep.* **2015**, *5*, 8457.

DOI: 10.1021/acs.jcim.7b00188
J. Chem. Inf. Model. 2017, 57, 1474−1487